Supplementary Information

High-performance, Acid-durable Nonprecious Ternary Alloy Cathode via Zn Dealloying for Proton Exchange Membrane Water Electrolysis

Chan Hee Lee, †[a] Kyeong-Rim Yeo †[a] and Soo-Kil Kim *[a]

[a] School of Integrative Engineering, Chung-Ang University, 84 Heukseok-ro, Dongjak-gu, Seoul 06974, Republic of Korea

† Contributed equally

*Corresponding author.

E-mail addresses: sookilkim@cau.ac.kr

1. Materials and methods

1.1 Catalyst preparation

NiMoZn catalysts were prepared via electrodeposition. All electrodeposition experiments were conducted in a homemade Teflon cell utilizing a three-electrode system under ambient temperature and pressure. A saturated calomel electrode (SCE, CHI 150) and graphite rod served as the reference and counter electrodes, respectively. Carbon paper (Ballard, Avcarb MGL280) with an exposed geometric area of 1.43 cm^2 was used as the working electrode. The electrolyte solution was prepared by dissolving $C_6H_5Na_3O_7 \cdot 2H_2O$ (7555-4405, Daejung), $ZnCl_2 \cdot 4H_2O$ (8597-4405, Daejung), $Na_2MoO_4 \cdot 2H_2O$ (7598-4405, Daejung), and $NiCl_2 \cdot 6H_2O$ (14-01045, Wako) in 40 mL of deionized water (18.2 MΩ·cm), followed by stirring for 20 min. To remove dissolved oxygen, N_2 gas was bubbled through the electrolyte for 30 min before deposition. Electrodeposition was performed using a potentiostat (CS350, Wuhan CorrTest Instrument Corp., Ltd.) by applying a constant potential at $-2\ V_{SCE}$ for 30 min. Following electrodeposition, the catalyst-coated carbon paper was dried under N_2 flow. The pristine NiMoZn (P-NiMoZn) catalyst was subsequently subjected to an electrochemical dealloying process to obtain the dealloyed NiMoZn (D-NiMoZn) catalyst. Dealloying was performed by applying a constant potential of $-0.45\ V_{SCE}$ for 1 h in 0.5 M H_2SO_4. To enhance the durability of the dealloyed catalyst in acidic environments, a post-heat treatment was performed at 400 °C for 2 h in a 4% H_2/Ar atmosphere, yielding the HD-NiMoZn catalyst.

1.2 Material characterization

The surface morphology of the catalysts was characterized using field emission scanning electron microscopy (FE-SEM, Zeiss Sigma). The bulk composition of the electrodeposited catalysts was analyzed by energy dispersive X-ray spectroscopy (EDS, Noran System 7, Thermo Fisher). The bulk crystalline structure of the catalysts was evaluated using X-ray diffraction (XRD, NEW D8-Advance, Bruker-AXS) in the 2θ range of 20°–80° at a scan rate of 1° min^{-1}. X-ray photoelectron spectroscopy (XPS, K-alpha+, Thermo Fisher Scientific) was performed to investigate the electronic structure, oxidation states, and surface composition of the catalysts. All binding energies obtained from XP spectra were calibrated with respect to the C 1s C–C peak at 284.8 eV.

1.3 Electrochemical characterization

The hydrogen evolution reaction (HER) activity was evaluated through cyclic voltammetry conducted in the potential range of −0.23 to 0.07 V_{RHE} at a scan rate of 1 mV s^{-1}. All HER polarization curves were corrected for iR drop using the ohmic resistance values obtained via electrochemical impedance spectroscopy (EIS). The electrochemical double-layer capacitance was determined through linear sweep voltammetry (LSV) conducted in the non-faradaic region of a 1 M NaOH electrolyte at scan rates ranging from 10 to 100 mV s^{-1}. The C_{dl} value was divided by the specific capacitance (C_s) of 40 µF cm^{-2} to obtain the roughness factor, and the HER current density was divided by the roughness factor to calculate the specific activity. Charge transfer resistance was analyzed via EIS at an overpotential of 30 mV, within a frequency range of 10^5 to 10^2 Hz, and an amplitude of 5 mV. Accelerated degradation tests (ADTs) were performed over 5,000 cycles between −0.2 and 0.05 V_{RHE} at a scan rate of 100 mV s^{-1}.

The durability of the catalysts was further evaluated under galvanostatic conditions at a constant current density of −10 mA cm^{-2} for 24 h. All electrochemical measurements were performed in a three-electrode system using 0.5 M H_2SO_4 as the electrolyte.

1.4 PEMWE performance measurements

The membrane electrode assembly (MEA) was fabricated using the HD-NiMoZn/CP catalyst, which exhibited optimal HER activity and durability, as the cathode with an active area of 1 cm^2. The anode was prepared by spray coating a commercial iridium oxide catalyst (043396, Alfa Aesar) with a loading of 2.0 mg cm^{-2} onto a carbon paper substrate. A Nafion 212 membrane (DuPont™, thickness 50.8 μm) was used as the proton exchange membrane without hot pressing. During PEMWE operation, the cell temperature was maintained at 90 °C, whereas the anode line was maintained at 95 °C, with deionized water supplied to the anode at a flow rate of 15 mL min^{-1}. PEMWE cell performance was evaluated after activation at 2.2 V_{cell} for 30 min, followed by a stepwise potential sweep from 2.2 to 1.35 V_{cell} in 0.05 V_{cell} increments, holding each step for 1 min. This protocol was repeated five times. The durability of the PEMWE cell was assessed at a constant current density of 1 A cm^{-2} for 50 h.

Table S1. Surface elemental compositions of P-$Ni_{81.6}Mo_{2.4}Zn_{16.0}$ and D-$Ni_{85.9}Mo_{3.3}Zn_{10.8}$ species after dealloying measured by EDS and XPS.

P-$Ni_{81.6}Mo_{2.4}Zn_{16.0}$	**Ni**	**Mo**	**Zn**
EDS atomic %	81.6	2.4	16.0
XPS atomic %	35.0	4.0	61.0
D-$Ni_{85.9}Mo_{3.3}Zn_{10.8}$	**Ni**	**Mo**	**Zn**
EDS atomic %	85.9	3.3	10.8
XPS atomic %	71.4	10.9	17.7

Table S2. Comparison of HER activity and PEMWE performance of HD-$Ni_{86.7}Mo_{3.2}Zn_{10.1}$ with commercial Pt/C. The Pt/C data used for comparison were taken from our group's previous publication.[1]

Catalyst	Overpotential / mV @ –10 mA cm^{-2}	Overpotential / mV @ –50 mA cm^{-2}
HD-$Ni_{86.7}Mo_{3.2}Zn_{10.1}$/CP	15.7	28
Pt/C	5.5	27.5

Membrane electrode assembly(MEA)	Temperature / °C	Current density / A cm^{-2} @ 2.0 V_{cell}	Cell Voltage / V_{cell} @ 1 A cm^{-2}
Cathode : HD-$Ni_{86.7}Mo_{3.2}Zn_{10.1}$ Membrane : Nafion 212 (50.8 µm) Anode : Com. IrO_x (2.0 mg cm^{-2})	90	1.897	1.819
Cathode : Pt/C/CP (0.05 mg cm^{-2}) Membrane : Nafion 212 (50.8 µm) Anode : Com. IrO_x (2.0 mg cm^{-2})	90	2.052	1.700

Table S3. HER activity and durability of HD-$Ni_{86.7}Mo_{3.2}Zn_{10.1}$ and previously reported nonprecious electrocatalysts and corresponding conditions in acidic electrolytes.

Catalyst	Overpotential @ –10 mA cm^{-2}	Tafel slope (mV dec^{-1})	Substrate	Electrolyte	Durability	Reference
HD-$Ni_{86.7}Mo_{3.2}Zn_{10.1}$	15.7	36	Carbon paper	0.5 M H_2SO_4	0.05 to –0.2 V_{RHE} @ 5k cycles 100 h @ –10 mA cm^{-2}	This study
$Cu_{44.4}Ni_{46}Mo_{9.6}$	18	27.7	Carbon paper	0.5 M H_2SO_4	–0.2 to –0.5 V_{SCE} @ 5k cycles 24 h @ –10 mA cm^{-2}	[2]
Nb-WSe_2	27	33.4	W mesh	0.5 M H_2SO_4	100 h @ 1000 mA cm^{-2}	[3]
FeP	144	76	Cu NW/CP	0.5 M H_2SO_4	100 h @ -100 mA cm^{-2}	[4]
Mo_3S_{13}-NCNT	188	40	GC RDE (1000 rpm)	0.5 M H_2SO_4	N/A	[5]
FeP/CP	38	34.8	Carbon paper	0.5 M H_2SO_4	90 h @ –10 mA cm^{-2}	[6]
defect-rich 1 T-2 H MoS_2NS/CFP	192	44	CFP	0.5 M H_2SO_4	38 h @ –10 mA cm^{-2}	[7]
$WO_{2.9}$/CP	169	48	Carbon paper	0.5 M H_2SO_4	0 to –0.2 V_{RHE} @ 1k cycles 10 h @ –10 mA cm^{-2}	[8]
10%Mn-MoS_2/CP	148	55	Carbon paper	0.5 M H_2SO_4	0.05 to –0.15 V_{RHE} @ 2k cycles	[9]
Co-MoS_2@CN	137	46.5	CN	0.5 M H_2SO_4	24 h @ –10 mA cm^{-2}	[10]
CoS_2/WS_2	79	52	Co_3O_4 skeleton	0.5 M H_2SO_4	0 to 0.5 V_{RHE} @ 1k cycles 50 h @ 100 mA cm^{-2}	[11]
MoO_2@CoMo	43	50	Carbon paper	0.5 M H_2SO_4	10 h @ –50 mA cm^{-2}	[12]
1T-$MoTe_2$/CC	211	73	Carbon cloth	1 M H_2SO_4	N/A	[13]
Ni@NCW	158	75	Carbonized wood	0.5 M H_2SO_4	3k cycles 100 h @ 500 mA cm^{-2}	[14]
FeMoS/C/CP	140	57	Carbon paper	0.5 M H_2SO_4	70 h @ –10 mA cm^{-2}	[15]
MoS_2:C = 1:3	70	72	Carbon cloth	0.5 M H_2SO_4	2k cycles	[16]

Table S4. PEMWE performance of HD-$Ni_{86.7}Mo_{3.2}Zn_{10.1}$ and previously reported nonprecious cathodes.

Membrane electrode assembly (MEA)			Temperature / °C	Current density / A cm^{-2}	Cell Voltage / V_{cell}	Reference
Cathode	Membrane	Anode		@ 2.0 V	@ 1 A cm^{-2}	
HD-$Ni_{86.7}Mo_{3.2}Zn_{10.1}$/CP	Nafion 212	Com. IrO_x/CP	90	1.897	1.817	This study
WMoC NA/CFP	Nafion 212	Com. IrO_2/ Pt coated sintered Ti	80	2.789	1.776	[17]
$Cu_{44.4}Ni_{46}Mo_{9.6}$/CP	Nafion 212	ED-IrO_2/CP	90	2.528	1.791	[2]
PANI/Ni_2P/CP	Nafion 117	IrO_2/Ti plate	80	2.026	1.822	[18]
NiMo/CF/CP	Nafion 212	ED-IrO_2/CP	90	1.96	1.837	[3]
$Ni_{96}W_4$/Cu NW	Nafion 212	ED-IrO_2/CP	90	1.79	1.877	[4]
M-$CoSe_{1.28}S_{0.72}$/Ti felt	Nafion 115	IrO_2/Pt coated Ti felt	60	1.523	1.79	[19]
Mo_3S_{13}-NCNT	Nafion 212	IrO_2/sintered Ti PTL	80	1.481	1.92	[5]
FeP/CP	Nafion 212	ED-IrO_2/CP	90	1.48	1.904	[6]
L-$Ni_{46}P_{54}$/CP	Nafion 212	ED-IrO_2/CP	90	1.47	1.936	[20]
defect-rich 1 T-2 H MoS_2NS/CFP	Nafion 115	$IrRuO_x$/LGDL	90	1.311	1.91	[7]
$WO_{2.9}$/CP	Nafion 117	Com. IrOx/ Ti felt	80	1.05	1.981	[8]
10%Mn-MoS_2/CP	Nafion 115	RuO_2 nanoparticles /CP	80	0.8	2.055	[9]
WC@NC/CP	Nafion 212	IrO_2/CP	80	0.78	-	[21]
Co-MoS_2/CP	Nafion 115	IrO_2/Ti mesh	80	0.737	2.106	[22]
$Cu_{93.7}Mo_{6.3}$/CP	Nafion 212	ED-IrO_2/CP	90	0.73	-	[10]
$Ni_{0.64}Co_{0.36}OxS_{0.28}$ /CP	Nafion 212	ED-IrO_2/CP	90	0.72	2.021	[11]
MoO_2@CoMo/CP	Nafion 212	ED-IrO_2/CP	90	0.62	-	[12]
MoS_x/CP	Nafion 212	ED-IrO_2/CP	90	0.57	-	[23]
NiP_2/ Ti fiber felt	Nafion 115	IrO_2/ Ti fiber felt	80	0.55	2.15	[24]

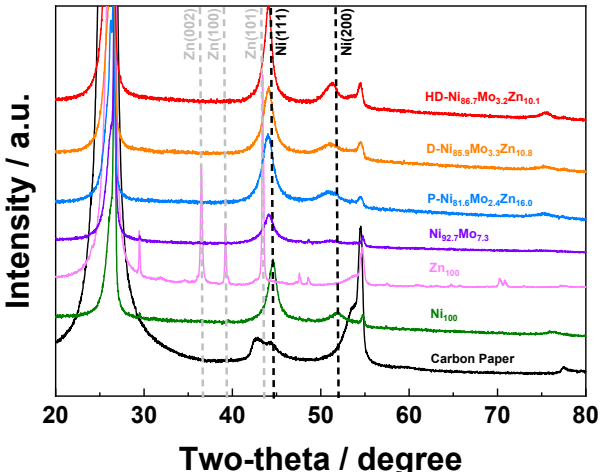

Figure S1. XRD patterns of Ni_{100}, Zn_{100}, $Ni_{92.7}Mo_{7.3}$, P-$Ni_{81.6}Mo_{2.4}Zn_{16.0}$, D-$Ni_{85.9}Mo_{3.3}Zn_{10.8}$, and HD-$Ni_{86.7}Mo_{3.2}Zn_{10.1}$.

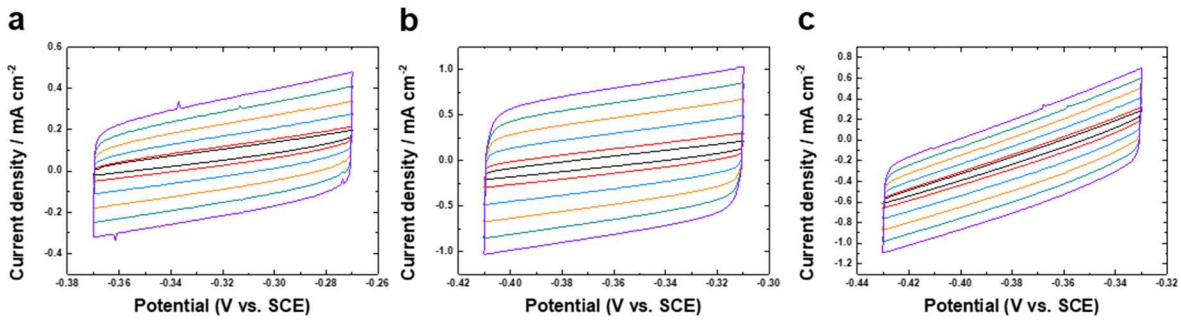

Figure S2. Electrochemical double-layer capacitance measurements for (a) P-$Ni_{81.6}Mo_{2.4}Zn_{16.0}$, (b) D-$Ni_{85.9}Mo_{3.3}Zn_{10.8}$, and (c) HD-$Ni_{86.7}Mo_{3.2}Zn_{10.1}$.

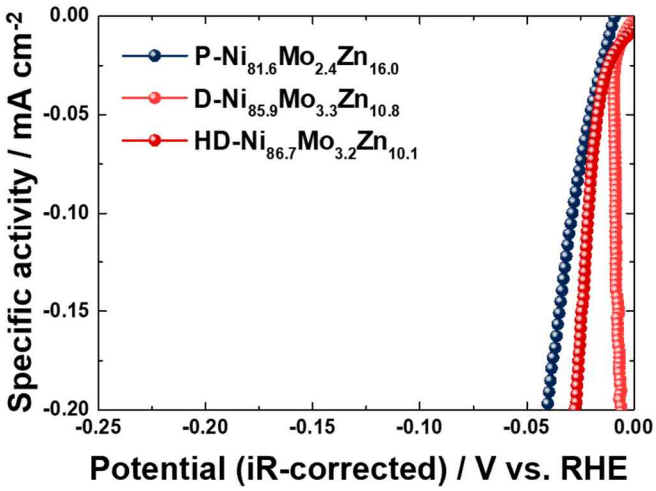

Figure S3. Specific activity for P-$Ni_{81.6}Mo_{2.4}Zn_{16.0}$, D-$Ni_{85.9}Mo_{3.3}Zn_{10.8}$, and HD-$Ni_{86.7}Mo_{3.2}Zn_{10.1}$.

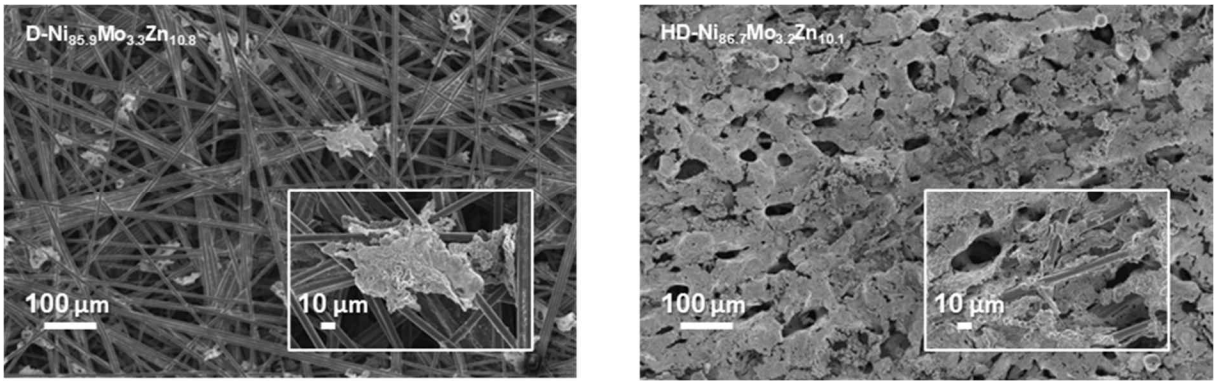

Figure S4. Characterization results after 5,000 CV cycles. FE-SEM images of D-$Ni_{85.9}Mo_{3.3}Zn_{10.8}$ and HD-$Ni_{86.7}Mo_{3.2}Zn_{10.1}$.

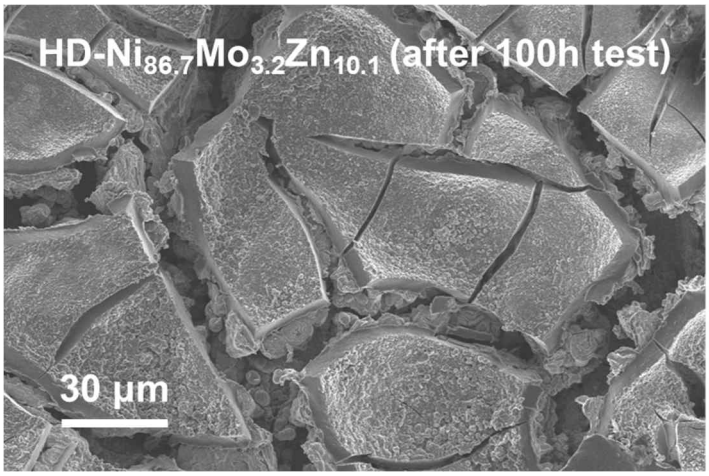

Figure S5. FE-SEM image of HD-$Ni_{86.7}Mo_{3.2}Zn_{10.1}$ after the 100 h stability test

References

1. K.-R. Yeo, H. Kim, K. S. Lee, S. Kim, J. Lee, H. Park and S.-K.Kim, *Applied Catalysis B: Environment and Energy*, 2024, *346*, 123738.
2. K. J. Choi, H. Kim and S.-K. Kim, *Journal of Power Sources*, 2021, 506, 230200.
3. X. Zhang, C. Yang, D. Zhou, D. Zhang, J. Zhang, and Z. Wang, *Journal of Alloys and Compounds*, 2025, 1051, 185708.
4. Y. Park and D.-H. Ha, *International Journal of Hydrogen Energy*, 2025, *136*, 392-401.
5. P. K. Holzapfel, M. Buehler, D. Escalera-López, M. Bierling, F. D. Speck, K. J. Mayrhofer, S. Cherevko, C. V. Pham and S. Thiele, *Small*, 2020, 16, 2003161.
6. Y. Park, H. Kim, T. Lee, Y.-K. Hong, W. Jeong, S.-K. Kim and D.-H. Ha, *Chemical Engineering Journal*, 2022, 431, 133217.
7. Z. Xie, S. Yu, X. Ma, K. Li, L. Ding, W. Wang, D. A. Cullen, H. M. Meyer III, H. Yu and J. Tong, *Applied Catalysis B: Environmental*, 2022, 313, 121458.
8. M. R. Qu, Y. R. Cheng, H. L. Duan, Y. Y. Qin, S. H. Feng, X. Z. Su, Y. F. Yuan, W. S. Yan, L. Cao and J. Xu, *Small*, 2024, 20, 2401159.
9. M. Rafei, A. Piñeiro-García, X. Wu, D. K. Perivoliotis, T. Wågberg and E. Gracia-Espino, *Materials Today Energy*, 2024, 41, 101524.
10. Z. Huang, J. Li, S. Guo, J. Liu, J. Zeng, and F. Yuan, *Separation and Purification Technology*, 2025, *354*, 129011.
11. C. Yao, Q. Wang, C. Peng, R. Wang, J. Liu, N. Tsidaeva, and W. Wang, *Chemical Engineering Journal*, 2024, *479*, 147924.
12. G. H. Han, H. Kim, J. Kim, J. Kim, S. Y. Kim and S. H. Ahn, *Applied Catalysis B: Environmental*, 2020, 270, 118895.
13. A. Kumar Samuel, A. H. Faqeeh, W. Li, Z. Ertekin, Y. Wang, J. Zhang, N. Gadegaard, D. A. Moran, M. D. Symes and A. Y. Ganin, *ACS Sustainable Chemistry & Engineering*, 2024, 12, 1276-1285.
14. D. Li, H. Cheng, X. Hao, G. Yu, C. Qiu, Y. Xiao and B. Zhang, *Advanced Materials*, 2024, *36*(4), 2304917.
15. A. Morozan, H. Johnson, C. Roiron, G. Genay, D. Aldakov, A. Ghedjatti, C. T. Nguyen, P. D. Tran, S. Kinge and V. Artero, *Acs Catalysis*, 2020, 10, 14336-14348.
16. J. Li, R. Miró, A. Wrzesińska-Lashkova, J. Yu, J. Arbiol, Y. Vaynzof, A. Shavel and V. Lesnyak, *Advanced Functional Materials*, 2024, 34, 2404565.
17. L. Shen, Y. Shi, T. O. Ogundipe, K. Huang, S. Cao, Z. Lu, Z. Wang, H. Tan and C. Yan, *Journal of Power Sources*, 2022, 538, 231557.
18. H. Shi, J. Qian and X. Hu, *Journal of Power Sources*, 2024, 596, 234099.
19. X.-L. Zhang, P.-C. Yu, X.-Z. Su, S.-J. Hu, L. Shi, Y.-H. Wang, P.-P. Yang, F.-Y. Gao, Z.-Z. Wu and L.-P. Chi, *Science Advances*, 2023, 9, eadh2885.
20. J. Kim, J. Kim, H. Kim and S. H. Ahn, *ACS Applied Materials & Interfaces*, 2019, 11, 30774-30785.
21. Q. Feng, Y. Xiong, L. Xie, Z. Zhang, X. Lu, Y. Wang, X.-Z. Yuan, J. Fan, H. Li and H. Wang, *ACS Applied Materials & Interfaces*, 2019, 11, 25123-25132.
22. J. Mo, S. Wu, T. Lau, R. Kato, K. Suenaga, T.-S. Wu, Y.-L. Soo, J. Foord and S. Tsang, *Materials Today Advances*, 2020, 6, 100020.
23. J. H. Kim, H. Kim, J. Kim, H. J. Lee, J. H. Jang and S. H. Ahn, *Journal of Power Sources*, 2018, 392, 69-78.
24. C. Hu, F. Ding, C. Lv, L. Zhou, N. Zeng, A. Liu, J. Cai and T. Tang, *Separation and Purification Technology*, 2025, 352, 128249.